

# Mapping the Human miRNA Interactome by CLASH Reveals Frequent Noncanonical Binding



Cell

# Mapping the Human miRNA Interactome by CLASH Reveals Frequent Noncanonical Binding

Aleksandra Helwak,[1,2] Grzegorz Kudla,[1,2,3] Tatiana Dudnakova,[1] and David Tollervey[1,*]
[1]Wellcome Trust Centre for Cell Biology, The University of Edinburgh, Edinburgh EH9 3JR, UK
[2]These authors contributed equally to this work
[3]Present address: MRC Human Genetics Unit, Institute of Genetics and Molecular Medicine, The University of Edinburgh, Edinburgh EH4 2XU, UK
*Correspondence: d.tollervey@ed.ac.uk
http://dx.doi.org/10.1016/j.cell.2013.03.043

## SUMMARY

MicroRNAs (miRNAs) play key roles in gene regulation, but reliable bioinformatic or experimental identification of their targets remains difficult. To provide an unbiased view of human miRNA targets, we developed a technique for ligation and sequencing of miRNA-target RNA duplexes associated with human AGO1. Here, we report data sets of more than 18,000 high-confidence miRNA-mRNA interactions. The binding of most miRNAs includes the 5′ seed region, but around 60% of seed interactions are noncanonical, containing bulged or mismatched nucleotides. Moreover, seed interactions are generally accompanied by specific, nonseed base pairing. 18% of miRNA-mRNA interactions involve the miRNA 3′ end, with little evidence for 5′ contacts, and some of these were functionally validated. Analyses of miRNA:mRNA base pairing showed that miRNA species systematically differ in their target RNA interactions, and strongly overrepresented motifs were found in the interaction sites of several miRNAs. We speculate that these affect the response of RISC to miRNA-target binding.

## INTRODUCTION

MicroRNAs (miRNAs) play a key role in the posttranscriptional regulation of gene expression by guiding the association between the RNA-induced silencing complex (RISC) and target RNAs (reviewed in Fabian et al., 2010). Human cells express more than 1,000 miRNAs, each potentially binding to hundreds of messenger RNAs (mRNAs) (Lewis et al., 2005), but only a small fraction of these interactions has been validated experimentally. Experiments conducted throughout the last decade have established a set of canonical rules of miRNA-target interactions (reviewed in Bartel, 2009): (1) interactions are mediated by the "seed" region, a 6- to 8-nt-long fragment at the 5′ end of the miRNA that forms Watson-Crick pairs with the target; (2) nucleotides paired outside the seed region stabilize interactions but are reported not to influence miRNA efficacy (Garcia et al., 2011; Grimson et al., 2007); and (3) functional miRNA targets are localized close to the extremes of the 3′ UTRs of protein-coding genes in relatively unstructured regions (Grimson et al., 2007). Recently, RISC-binding sites on mRNAs have been mapped transcriptome wide by crosslinking, immunoprecipitation, and high-throughput sequencing (CLIP-seq), allowing prediction of many miRNA-mRNA interactions (Chi et al., 2009; Hafner et al., 2010a; Zhang and Darnell, 2011) and yielding data consistent with the canonical rules.

However, there is substantial evidence for exceptions to these rules. As examples, in *C. elegans*, the well-studied *lin-4::lin-14* interaction involves bulged nucleotides (Ha et al., 1996), whereas the *let-7::lin-41* interaction involves wobble G·U pairing (Vella et al., 2004). Human miR-24 targets important cell-cycle genes using interaction sites that are spread over almost the whole miRNA. These interactions lack obvious seed pairing and contain multiple mismatches, bulges, and wobbles (Lal et al., 2009). Analysis of the miR-124 targets recovered by HITS-CLIP revealed a mode of miRNA-mRNA binding that involves a G bulge in the target, opposite miRNA nucleotides 5 and 6. It has been estimated that about 15% of miR-124 targets in mice brain are recognized by this mode of binding (Chi et al., 2012). Another, apparently rare, base-pairing pattern called "centered site" (Shin et al., 2010) involves 11 consecutive Watson-Crick base pairs between the target and positions 4–14 or 5–15 of miRNA. There are also multiple exceptions regarding the requirement for miRNA-binding sites to be located in the 3′ UTR. Functional miRNA-binding sites have occasionally been reported in 5′ UTRs (Grey et al., 2010) and, more frequently, within mRNA coding sequences (Hafner et al., 2010a; Reczko et al., 2012). Moreover, recent reports show that miRNA targets are not limited to protein-coding transcripts and can be found in noncoding RNAs (ncRNAs) that arise from pseudogenes (Poliseno et al., 2010). Together, these data indicate that miRNAs can bind to a wide variety of targets, with both canonical and noncanonical base pairing, and indicate that miRNA targeting rules may be complex and flexible.

To allow direct, high-throughput mapping of RNA-RNA interactions, we previously developed crosslinking, ligation, and sequencing of hybrids (CLASH) (Kudla et al., 2011). High-throughput methods have been developed to map protein-DNA interactions, protein-RNA interactions, and DNA-DNA interactions, so CLASH completes the toolkit necessary to study nucleic acid interactomes. Here, we adapted CLASH to allow direct observation of miRNA-target pairs as chimeric reads in deep-sequencing data. Our transcriptome-wide data set reveals the prevalence of seed and nonseed interactions and the diversity of in vivo targets for miRNAs.

## RESULTS

### CLASH Directly Maps miRNA-Binding Sites

To recover RNA species bound to the human RISC complex, we created an N-terminal fusion of hAGO1 with a protein A-TEV cleavage site-$His_6$ tripartite tag (PTH-AGO1). N-terminally tagged AGO proteins were used previously in many studies and were shown to be functional (Chatterjee and Grosshans, 2009; Lian et al., 2009). Actively growing Flp-In T-REx 293 cells stably expressing PTH-AGO1 were UV irradiated (254 nm) to crosslink proteins to interacting RNAs. PTH-AGO1 was purified, and interacting RNA molecules were partially hydrolyzed, ligated, reverse transcribed, and subjected to Illumina sequencing. At the ligation step, RNA molecules present in AGO-associated miRNA-target duplexes can be joined together (Figure 1A). Following RT-PCR amplification, these generate "chimeric" complementary DNAs (cDNAs), which can be identified because they contain two regions that map to sites that are noncontiguous in the transcriptome sequence (Figure 1B).

When AGO1-associated RNAs were analyzed, around 98% were "single reads" representing AGO1-binding sites on RNAs, similar to those obtained with HITS-CLIP and PAR-CLIP (Chi et al., 2009; Hafner et al., 2010a). However, ~2% were chimeric reads reflecting intermolecular stem structures present in the AGO1-associated RNAs (Figures 1A and 1B). Supporting the significance of the chimeras, 94% of the sequences involved were also recovered as single reads in at least one experiment (Figure 1C). As a control experiment, the lysate obtained from UV-irradiated human cells was mixed with an equal quantity of yeast lysates prior to CLASH analysis (details in Extended Experimental Procedures and Table S2C). This revealed that the background arising from RNA-RNA interactions formed in vitro represents <2% of single and chimeric reads, confirming that interactions recovered by CLASH were predominately formed in vivo.

Six independent experiments (E1–E6) were performed with slightly differing protocols, yielding broadly comparable data that were analyzed together (Figure S1 and Tables S1 and S2A available online). mRNAs form the principal class of miRNA binding partners identified in chimeric reads and constitute nearly 70% of interactions (Figure 1D). Other known target classes were recovered, including pseudogenes and long-intergenic ncRNAs (lincRNAs), as were substantial numbers of chimeras with ribosomal RNAs (rRNAs), transfer RNAs (tRNAs), small nuclear RNAs (snRNAs), and miRNAs. The 18,514 miRNA-mRNA interactions identified from chimeric reads were analyzed in detail. These represent 399 different miRNAs and 6,959 different protein-coding genes (Table S2B). The full set of miRNA-mRNA chimeras identified is included in Data S1.

### Validation of Interactions Identified by CLASH Supports Their Reliability

To assess whether the interactions identified are functionally important, we determined whether they (1) resemble known and predicted miRNA-mRNA interactions, (2) show evolutionary conservation, and (3) are associated with downregulation of target genes.

The CLASH data set included a number of previously known interactions (Table S3). For example, the association between miR-196a/b and transcripts from the *HOX* gene family (*HOXB8* and *HOXC8*) (Yekta et al., 2004) (Figure 1C) was found in five of six CLASH experiments and was supported by 275 chimeric reads. In addition to the known interaction in the 3′ UTR of *HOXC8*, we identified a miR-196 interaction in the 5′ UTR. In contrast, interactions involving liver-specific miR-122 or brain-specific miR-124 were strongly depleted, highlighting the tissue specificity of the miRNA interactome recovered by CLASH from HEK cells.

To estimate the overlap between the CLASH targets (i.e., interactions identified in miRNA-mRNA chimeras) and experimentally determined AGO-binding sites in mRNAs, we compared chimeras and single reads from the present study. 94% of CLASH targets were identified as AGO1-binding sites in the nonchimeric reads; 3,066 of these (16.6% of all) were high-confidence clusters of 20 or more distinct nonchimeric reads. In addition, 1,596 CLASH targets coincided with high-confidence AGO1-4-binding sites previously mapped by PAR-CLIP in HEK293 cells (Hafner et al., 2010a), a 3-fold enrichment over expected chance levels for expression-matched transcripts (Table S4A). CLASH targets were also compared to sets of miRNA targets bioinformatically predicted by the programs miRanda (John et al., 2004), PicTar (Krek et al., 2005), PITA (Kertesz et al., 2007), RNAhybrid (Rehmsmeier et al., 2004), and TargetScan (Lewis et al., 2005) (Table S4B). This analysis was limited to CLASH targets located in 3′ UTRs of human RefSeq transcripts because published predictions are generally restricted to these regions. CLASH targets were highly enriched (average 14-fold) in the predicted data compared to controls. These findings strongly indicate that chimeras faithfully reflect in vivo miRNA-mRNA interactions.

Many characterized miRNA interactions involve perfect complementarity between the miRNA 5′ region, particularly nucleotides 2–8 (known as the seed sequence) and the target RNA. Comparison to randomized sequences showed strong enrichment for exact (Watson-Crick, "canonical seed") and near-exact (G·U pairs, up to one nt mismatch or bulge; "noncanonical seed") 6-mer seed matches among chimeras (Figure 2A). Notably, noncanonical seed interactions were ~1.7-fold more common than perfect base pairing.

Binding energies for the miRNA-mRNA interactions were predicted from in silico folding of sequences recovered in chimeras and compared to predicted binding energies in several control data sets (Figures 1B and 2B). This showed that miRNA-mRNAs chimeras recovered are strongly enriched

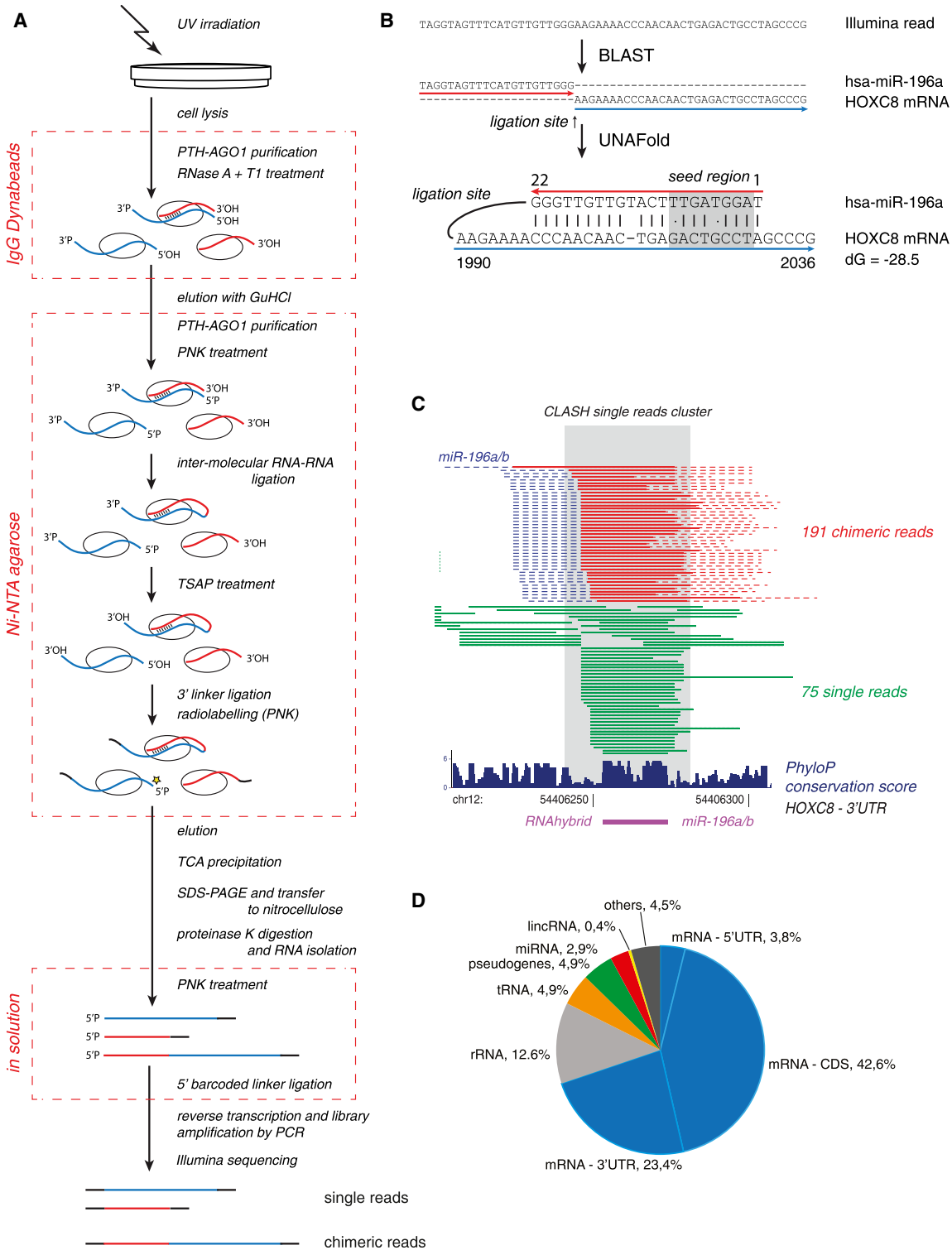


**Figure 1. Overview of Experimental and Bioinformatic Procedures**

(A) Growing cells were UV irradiated, and PTH-AGO1 was purified. RNA fragmentation, ligation, cDNA synthesis, and sequencing of AGO1-associated RNAs allowed the identification of sites of AGO1 binding (as single reads) and RNA-RNA interactions at AGO1-binding sites (as chimeric reads).

(B) Sequencing reads were mapped to a database of human transcripts using BLAST (Altschul et al., 1990). Sequences reliably mapped to two different sites were folded in silico using UNAFold (Markham and Zuker, 2008) to identify the interaction site of the RNA molecules that gave rise to the chimeric cDNA.

*(legend continued on next page)*

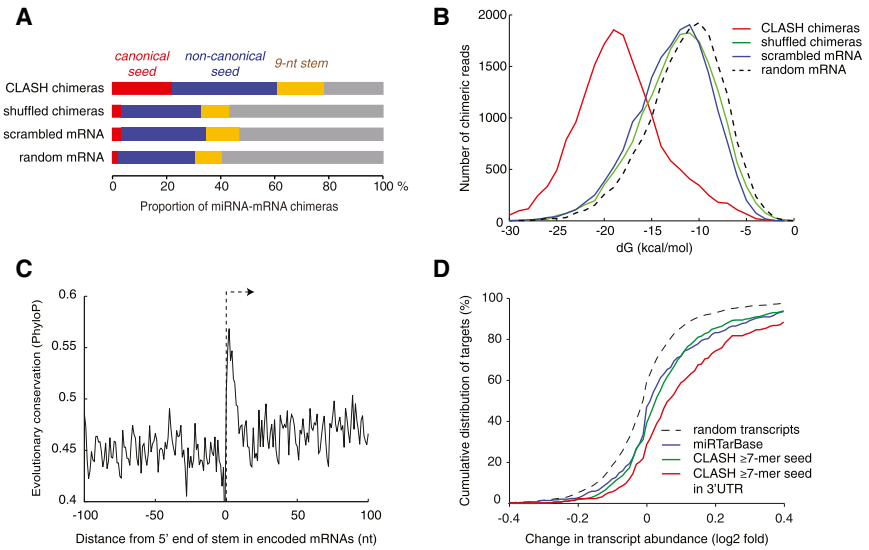


**Figure 2. Bioinformatic and Experimental Validation of miRNA-mRNA Interactions**

(A) Proportion of canonical seed interactions (exact Watson-Crick pairing of nts 2–7 or 3–8 of the miRNA), noncanonical seed interactions (pairing in positions 2–7 or 3–8, allowing G-U pairs and up to one bulged or mismatched nucleotide), or 9 nt stems (allowing bulged nucleotides in the target) among CLASH chimeras and several randomized data sets; the differences between CLASH and randomized data sets were highly significant (chi-square tests, $p < 10^{-300}$, $p < 10^{-100}$, and $p < 10^{-80}$ for canonical seeds, noncanonical seeds, and stems, respectively).

(B) The mean predicted binding energy between miRNA and matching target mRNA found in chimeras was stronger by over 5 kcal $mol^{-1}$ than in randomly matched pairs (t test, $p < 10^{-300}$).

(C) Average conservation score along mRNA 3′ UTRs, centered at the 5′ end of the longest stem predicted within each CLASH target. The mean conservation score within predicted stems was significantly higher than in flanking regions of the 3′ UTR (0.54 versus 0.46, t test, $p < 10^{-26}$, n = 4634).

(D) Changes in mRNA abundance following the depletion of 25 miRNAs (Hafner et al., 2010a). The graph shows a cumulative distribution of the log2 fold change (LFC) of mRNA abundance upon miRNA depletion for different sets of mRNAs: targets of the 25 miRNAs identified by CLASH with a 7-mer seed match (green line), CLASH targets in the 3′ UTR with 7-mer seed match (red line), targets extracted from the miRTarBase (blue line), and random transcripts with expression levels matching the CLASH targets (dashed line). Displacement of the curve to the right reveals increased abundance following miRNA depletion, which is indicative of mRNA repression in the presence of the tested miRNAs.

See also Figure S2; Tables S3, S4A, and S4B; and Data S1.

for stably base-paired interactions. The strong binding energies of chimeric reads indicate that these result from genuine RNA-RNA interactions rather than from proximity-induced ligation of noninteracting RNAs in solution. Fitting a Gaussian mixture model to the observed distribution of binding energies (Figure S2A) suggested the existence of two populations; 89% of miRNA-mRNAs duplexes recovered having a lower energy distribution than the remaining 11%. Weak interactions may be disfavored in the recovered chimeras due to loss during sample preparation. However, exact interactions are typically slightly stronger than near-exact interactions (−19.4 kcal $mol^{-1}$ versus −18.6 kcal $mol^{-1}$), so any bias in the CLASH method will favor exact interactions. Thus, the expected direction of bias does not explain the high numbers of near-exact interactions identified.

Evolutionary conservation has been widely used to identify miRNA-binding sites. To quantify the conservation of putative miRNA-target interactions identified by CLASH, we analyzed PhyloP conservation scores (Pollard et al., 2010) within targets mapped to 3′ UTRs of annotated mRNAs from 46 vertebrate genomes. The identified miRNA target sites showed marked conservation relative to flanking regions, supporting their biological importance (Figure 2C). Because the CLASH technique depends on the recovery and sequencing of cross-linked RNA, the results will be biased by transcript abundance. Comparison of the distribution of CLASH targets to mRNA abundance (Figure S2B) revealed enrichment for more abundant targets, as expected. However, even relatively low abundance targets are well represented in the data set, showing that the CLASH approach is not limited to abundant mRNAs.

Interactions with miRNAs frequently result in downregulation of target mRNAs. To functionally validate CLASH targets, we reanalyzed published data reporting the effects of simultaneous depletion of 25 different miRNAs on mRNA levels (Hafner et al., 2010a). The expectation is that miRNA depletion will increase the abundance of target RNAs due to loss of repression. Cognate miRNA-mRNA pairs identified by CLASH and represented in the miRNA depletion data set were retrospectively analyzed and compared to confirmed miRNA-mRNA pairs from miRTarBase (Hsu et al., 2011). Similar upregulation was observed among the CLASH targets with a canonical 7-mer seed and validated miRTarBase targets (Figure 2D). In agreement with previous findings, upregulation was highest among those targets that contained a seed match and were located in the 3′ UTR (Figures 2D and S2C–S2F). Targets lacking a canonical seed match were also upregulated, on average half as efficiently as the seed-containing targets (Figure S2F). Such interactions would not generally be identified by target prediction programs, which are biased toward canonical seed

(C) Example interaction between miR-196a/b and *HOXC8* that was supported by chimeric reads (red), and a cluster of nonchimeric reads (green). The blue dashed line represents the location of the miRNA bit of chimera, and the red dashed line shows the 25 nt mRNA extension added during the analysis. The interaction was previously shown experimentally (Li et al., 2010) and can be predicted by RNAhybrid (Rehmsmeier et al., 2004).

(D) Distribution of all miRNA interactions among various classes of RNAs. The main miRNA targets are mRNAs and are represented by 18,514 interactions.

See also Figure S1 and Tables S1 and S2A–S2C.

interactions, whereas our findings support their reliability. Targets in CDSs were significantly upregulated upon miRNA depletion ($p = 3.4 \times 10^{-10}$), and upregulation of sites in the CDS is about half of that in 3′ UTRs (Figure S2F). Comparisons across all predicted interactions did not reveal a clear correlation between predicted binding energy and target regulation (Figure S2D). Notably, cohorts of predicted miRNA-mRNA interactions outperform the experimentally confirmed interactions taken from miRTarBase when compared transcriptome wide for their effects on mRNA stability (Figures 2D and S2C).

## Analysis of miRNA-mRNA Base-Pairing Patterns Reveals the Prevalence of Nonseed Interactions

The large data set provided by AGO1-CLASH allowed the miRNA interactome to be characterized ab initio without utilizing prior knowledge of targets or binding modes. To re-evaluate the rules underlying miRNA interactions, we developed a graphical representation of miRNA-target RNA base pairing and applied K-means clustering to reveal five classes of interactions with distinct base-pairing patterns (Figures 3A and 3B and Data S2). Three of these classes (I–III) featured binding between the miRNA seed and the target but differed in the presence and positioning of additional base-paired nucleotides within the miRNA. Class I interactions are confined to the seed region, whereas classes II and III additionally involve miRNA nucleotides 13–16 and 17–21, respectively. In class IV, binding was limited to a region located in the middle and 3′ end of the miRNA, whereas class V showed distributed or less stable base pairing. The observed patterns of miRNA-mRNA interactions were largely absent among randomized pairs (Figures S3A and S3B). Evolutionary conservation and target downregulation were strongest in class II (Table 1), supporting the important role of 5′ and 3′ end base pairing in miRNA function (Broderick et al., 2011). The proportion of interactions that were supported by CLASH AGO1 single-read clusters or PAR-CLIP AGO1-4 binding clusters in mRNA was similar for each base pairing class (Figure 3C), suggesting that all classes are largely reliable.

Two-thirds of all miRNAs analyzed showed nonrandom distribution across the five base pairing classes. Most miRNAs, including let-7a, miR-10a, and miR-15b, were enriched in the seed-interacting classes I–III, but miR-92a and 11 other miRNAs showed highest enrichment in the nonseed class IV (Figure 3D). Comparison of the six different CLASH protocols indicated that protocol E4 yielded the largest proportion of chimeras in classes I–IV (Figure S3C).

## Analysis of Enriched Motifs on mRNA Targets Identifies the Major Interaction Site for Many miRNAs

To identify additional features of miRNA-binding sites, we sought statistically overrepresented sequence elements in the CLASH targets of each miRNA using MEME (Bailey and Elkan, 1994) (Figure 4A). For many miRNAs, highly enriched sequence motifs emerged. In the majority of cases, the motifs were complementary to the miRNA seed region; however, motifs found for several miRNAs indicated preferred interactions with the 3′ region of the miRNA (Figures 4B and 4C and Table S5). Different miRNAs seem to follow idiosyncratic patterns of complementarity, but some common features emerge. For example, all six variants of let-7 yield almost exactly the same enriched motif that maps to nucleotides 2–8 of the miRNA (Figure S4). Interestingly, the nucleotide predicted to base pair with the U at position 6 in let-7 is the most variable. This pattern resembles the characterized *let-7::lin-41* interaction and the G bulges recently identified in target sequences located opposite positions 5–6 in the miRNA (Chi et al., 2012).

Many miRNAs are highly conserved in evolution; regions of highest conservation are typically the seed element (nt 1–8) and a downstream region (nt 13–19) (Grimson et al., 2007). We compared the sequence conservation patterns for miRNAs associated with 5′ (seed) or 3′ (nonseed) motifs (Figure 4D). Both in the case of 5′ and 3′ binding motifs, the part of the miRNA that contains the motif shows stronger evolutionary conservation than the part without motif (paired t test, $p = 0.001$ and 0.002 for 5′ and 3′ motifs, respectively). The identified motifs might be favored because they improve the efficiency of target RNA interactions with the AGO1-miRNA complex or because they influence the effects of miRNA binding on the fate of the mRNA. The identified motifs showed a higher average GC content than seed regions, suggesting selection for enhanced base pairing (Figure 4E).

## Experimental Validation of Noncanonical Interactions

To test the role of nonseed interactions in target regulation, we chose miR-92a that is abundant in HEK293 cells and shows clear preference toward 3′ end interactions (Figures 3D and 4B). We prepared reporter vectors by inserting potential target sequences into the 3′ UTR of *Renilla* luciferase (Figure 5A). Complementarity to only the seed region of miR-92a, to only the nonseed 3′ motif of miR-92a, or to both regions (S + M) each caused miR-92-dependent downregulation of luciferase expression. We have also analyzed five further reporters that included large fragments of 3′ UTRs of putative nonseed miR-92a targets. Four of these UTR regions contain no miR-92a seed matches (6 nt or longer), whereas one region contained a 7 nt seed match. All five reporters showed a statistically significant increase in expression on depletion of miR-92a (Figure 5B). This experiment shows that a nonseed interaction involving miR-92a can downregulate mRNA translation in the context of an entire 3′ UTR region.

To further test the ability of miR-92a to regulate various kinds of targets, miR-92a was depleted from HEK293 cells using specific inhibitors (Figure 5C), and the abundance of targets randomly selected from our data set matching either seed or nonseed 3′ motif was measured by qRT-PCR. miR-92a depletion resulted in increased abundance of 7/9 (78%) seed-matching targets and 7/11(63%) motif-matching targets.

We also quantified mRNA transcriptome wide using Affymetrix microarrays. We found that miR-92a targets with the 3′ motif (Figure 4B) were significantly upregulated after miR-92a depletion compared to genes not identified as miR-92a targets by CLASH ($p < 1 \times 10^{-6}$; Figures 5D and S5). Furthermore, mRNAs predicted to base pair with the 3′ end of miR-92a only (Figure 3B, cluster IV) are upregulated with respect

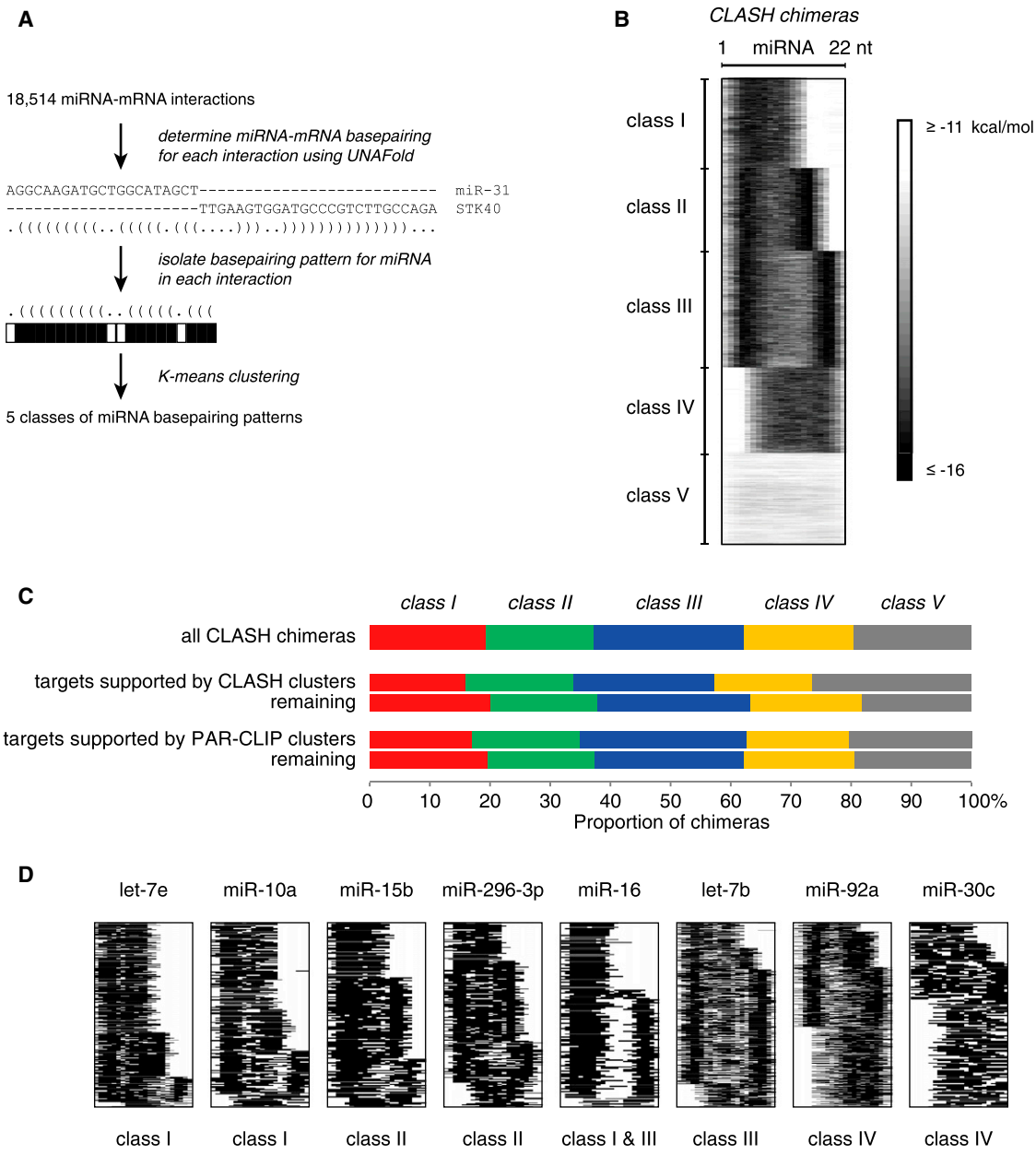


**Figure 3. Base-Pairing Patterns in miRNA-mRNA Interactions**

(A) Outline of the analysis of miRNA-mRNA base-pairing patterns. Unpaired nucleotides are in white, and paired nucleotides are in shades of gray depending on the overall interaction strength.

(B) Positions of base-paired nucleotides in miRNAs among the 18,514 miRNA-mRNA interactions. The names of interaction classes (I–V) are indicated.

(C) Distribution of CLASH targets among the five base-pairing classes. A similar proportion of CLASH targets from each class are supported by experimentally determined AGO-binding sites, as identified by CLASH single read clusters and PAR-CLIP clusters.

(D) Examples of miRNAs with nonrandom distribution across interaction classes. Of the 68 miRNAs tested, 31 were nonrandomly distributed across four classes of interaction ($p < 0.05$, chi-square test with Bonferroni correction; class V interactions were excluded from this analysis).

See also Figure S3 and Data S2.

to nontarget genes ($p < 1 \times 10^{-5}$). Although genes containing a miR-92a 7-mer seed match were upregulated relative to control, genes containing both a seed match and a cluster IV CLASH target were upregulated twice as highly ($p = 0.003$). Finally, genes containing a cluster IV CLASH target and no seed match were upregulated relative to genes containing neither a CLASH target nor a seed match ($p = 0.007$).

The CLASH data therefore identify a group of miRNAs that preferentially interact with their targets using nonseed regions.

**Table 1. Analysis of the Five miRNA-mRNA Base-Pairing Classes**

| Class | I | II | III | IV | V |
|---|---|---|---|---|---|
| Number of interactions | 3,594 | 3,293 | 4,630 | 3,389 | 3,608 |
| Number of base-paired nucleotides | 13.0 ± 0.04 | 15.3 ± 0.03 | 16.8 ± 0.03 | 14.6 ± 0.04 | 11.9 ± 0.05 |
| Number of base-paired nucleotides in seed | 5.2 ± 0.02 | 5.1 ± 0.02 | 5.0 ± 0.01 | 2.6 ± 0.02 | 3.3 ± 0.03 |
| Interaction energy (dG) | −18.3 ± 0.04 | −20.2 ± 0.06 | −20.5 ± 0.05 | −19.0 ± 0.05 | −11.1 ± 0.05 |
| PhyloP conservation score | 0.092 ± 0.017 | 0.127 ± 0.018 | 0.097 ± 0.017 | 0.011 ± 0.017 | 0.086 ± 0.018 |
| Efficiency of inhibition by miRNA | 0.042 ± 0.007 | 0.052 ± 0.009 | 0.047 ± 0.005 | 0.024 ± 0.005 | 0.039 ± 0.004 |
| Targets in 5′ UTR | 4.8% | 4.2% | 4.1% | 5.8% | 4.7% |
| Targets in CDS | 60.7% | 61.1% | 61.4% | 63.9% | 53.4% |
| Targets in 3′ UTR | 32.7% | 32.2% | 32.1% | 28.1% | 39.5% |

The number of predicted base pairs between the entire miRNA and the target or the miRNA seed region (nts 2–7) and the target was predicted using the RNAhybrid program from the UNAFold suite. The minimum free energy of interaction was calculated with RNAhybrid. The PhyloP conservation score was calculated as the difference between the average PhyloP score in the longest stem predicted in each interaction and the average PhyloP score in flanking genomic DNA (Pollard et al., 2010). The efficiency of target inhibition by miRNA was calculated as the average log2 fold enrichment of mRNA in miRNA-depleted versus control cells using published microarray data (Hafner et al., 2010a). The numbers in the table represent the mean with SE for each class of interactions. The proportion of targets in the 5′ UTR, CDS, and 3′ UTR was calculated using the annotations of ENST transcripts downloaded from Ensembl through Biomart. Overall, 60% of all targets were mapped to the coding sequence, and 35% were mapped to the 3′ UTR. The proportions of targets mapped to the 3′ UTRs are slightly lower compared to previous CLIP-seq experiments. We believe that this results from our method of mapping sequencing reads to a transcriptome database, which recovers reads mapped to splice junctions, thereby recovering more hits in coding sequences. When CLASH targets mapped to splice junctions are discarded, 50% of the remaining targets are mapped to the coding sequence, and 42% are mapped to the 3′ UTR.

Nonseed interactions have statistically significant but only modest effects on mRNA stability and/or translation.

### miRNAs Target ncRNAs

AGO was previously shown to associate with a wide range of RNA species (Burroughs et al., 2011). We reproducibly recovered chimeras between a subset of miRNAs and other miRNAs, tRNAs, snRNAs, lincRNAs, and rRNAs (Figure 1D). As initial validation of non-mRNA interactions, we assessed the effects of miR-92a depletion on the lincRNA AC012652-2 (Figure 6A). Depletion of miR-92a resulted in upregulation of the lincRNA to an extent similar to validated mRNA targets, supporting their functional interaction. Notably, recent work by the Rajewsky and Kjems groups has identified a lncRNA (CDR1as) that acts as an endogenous sponge for miR-7 (Hansen et al., 2013; Memczak et al., 2013). Hybrids between miR-7 and the CDR1as transcript were identified in our analysis (data not shown) supporting the presence of this interaction in vivo.

miRNA-miRNA interactions were also reproducibly recovered. As an example, Figure 6B shows the interaction between members of the let-7 and miR-30 families. The six let-7 miRNAs recovered each interacted with miR-30c and miR-30b, but no let-7 chimeras were identified with miR-30a. Although somewhat fewer single reads were recovered for miR-30a than for miR-30b or miR-30c, the lack of chimeras indicates that the interactions are not random.

Chimeras between $tRNA_{Lys}^{UUU}$ and miR-10a/b, miR125a/b, and miR193b were each recovered in several independent experiments (Figure 6C). $tRNA_{Lys}^{UUU}$ is required as a primer for genome replication by reverse transcriptase for HIV-1 and other lentiviruses (Barat et al., 1989). The most numerous and highly reproducible non-mRNA chimeras were found with the 18S and 28S rRNAs. Different miRNAs showed very distinct patterns of rRNA interaction. Some miRNA-binding sites were located in exposed, surface regions and could have formed on intact, functional ribosomes, whereas other sites are internal to the ribosomal subunits and may reflect interactions with preribosomes or degradation fragments. The interaction sites between miRNAs and all classes of non-protein-coding transcripts are listed in Data S3.

## DISCUSSION

The aim of this study was to obtain an unbiased view of the human miRNA interactome and to use the information to reevaluate the rules that govern miRNA-target base pairing. The 18,500 miRNA-mRNA interactions recovered provide a large data set of miRNA interactions that is independent of bioinformatic predictions. Multistep validation, which included structural, thermodynamic, evolutionary, and functional analysis, supports the reliability of our data. Moreover, a control CLASH experiment performed with mixed human and yeast lysates indicated that the large majority (>98%) of the miRNA-target RNAs interactions identified by CLASH had formed in vivo in human cells.

Although seed-mediated interactions constitute the largest class in our data, only around 37% of seed interactions involve uninterrupted Watson-Crick base pairing. This figure seemed surprisingly low but is consistent with the many observations of endogenous noncanonical miRNA targets. High-throughput studies found fewer noncanonical (or nonseed) interactions (Chi et al., 2009; Hafner et al., 2010b), but this may reflect an inherent bias in that seed binding was used to computationally identify interactions. Notably, many high-confidence AGO-binding sites identified in previous CLIP-seq data could not be assigned

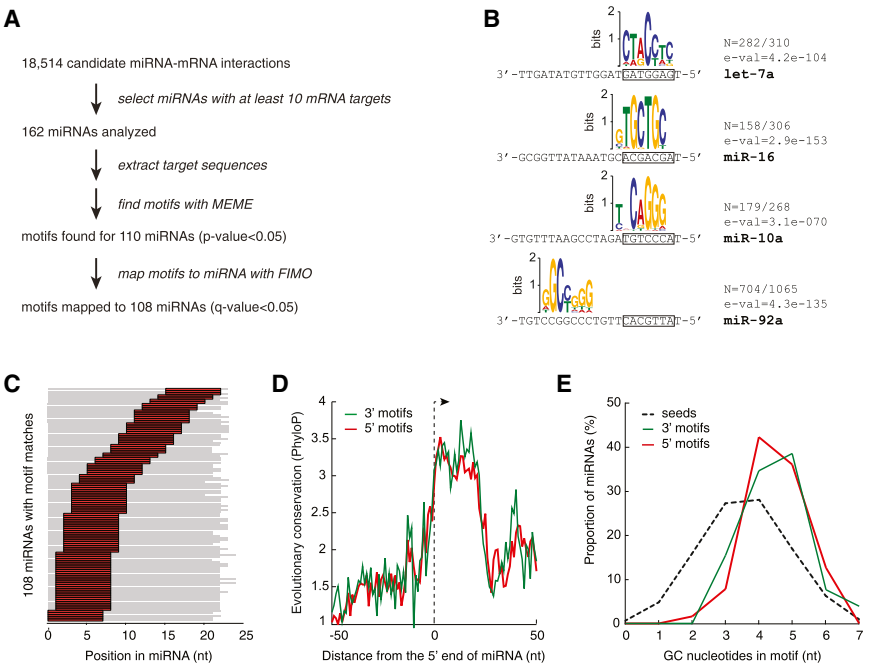


**Figure 4. Sequence Motifs Associated with miRNA-Binding Sites**

(A) Discovery pipeline for overrepresented motifs in miRNA targets. Target sequences with 25 nt flanking genomic sequence were analyzed by MEME (Bailey and Elkan, 1994), and 7-mer motifs were considered. 108 could be mapped back to the miRNA by FIMO (Grant et al., 2011) with FDR < 0.05.

(B) Example motifs bound by miRNA. n, number of motifs found/total number of targets analyzed. E-val, e-value of the motif returned by MEME. Most motifs are complementary to the miRNA seed (boxed).

(C) Distribution of conserved motif positions within 108 miRNAs. In most cases, the motifs enriched in miRNA targets were complementary to the miRNA seed (nt 1–9); however, some highly enriched motifs were complementary to regions in the middle or 3′ ends of the miRNA.

(D) Conservation patterns among 108 miRNAs with recognizable target motif sequences. miRNAs were partitioned by most enriched motif location into groups predicted to form seed and nonseed interactions. The 5′ half of the miRNA is more conserved among the seed-interacting group (average difference in PhyloP scores [Pollard et al., 2010] between 5′ and 3′ halves, $\Delta_{PhyloP} = 0.122$, t test, $p = 0.001$). The 3′ half of the miRNA is more conserved among the nonseed interacting group ($\Delta_{PhyloP} = -0.164$, $p = 0.002$).

(E) Distribution of GC content in motifs (n = 108) and miRNA seeds (n = 1100). The average guanine plus cytosine (GC) content of the binding motifs was higher than the average GC content of miRNA seeds in human.

See also Figure S4 and Table S5.

bioinformatically to any specific miRNA. Computational searches for miRNA-mRNA interactions have also been biased toward the identification of binding sites in 3′ UTR regions. In contrast, we observed substantial numbers of miRNA interactions in all the regions of mRNAs, with the greatest number of hits in coding sequences. Notably, different miRNAs vary in the relative proportions of targets in 5′ UTRs, coding sequences, and 3′ UTRs. As examples, miR-100 returned 4% 5′ UTR: 23% CDS: 73% 3′ UTR, whereas miR-149 returned 8% 5′ UTR: 72% CDS: 19% 3′ UTR (data not shown).

To provide an overview of the key features of miRNA-mRNA interactions, we analyzed miRNA base-pairing patterns by cluster analysis. As expected, the most frequent miRNA interaction site with a target is the seed, and base pairing in this region is detected for more than half of the interactions. However, seed interactions alone are found in only a relatively small fraction of identified targets (class I, 19%). Defined classes II–III agree with previously described 3′ supplementary and compensatory sites (Grimson et al., 2007; Lian et al., 2009). Unexpectedly, we identified a substantial class of interactions (class IV, 16% of all interactions) that does not involve contacts within the seed region and resembles reported "seedless" interactions (Lal et al., 2009). The identification of miRNAs that predominately interact with target mRNAs using their 3′ regions helps explain the pattern of evolutionary conservation of these miRNAs. However, target mRNAs that fall into this class seem to be relatively poorly conserved in evolution, and high-throughput data show that, on average, these targets respond only weakly to miRNA binding. Our experimental data on the regulation of miR-92a targets agree with this analysis, showing a statistically significant but moderate effect of class IV interactions on mRNA stability and possibly translation in reporter constructs. The results further suggested that the 3′ motif might act cooperatively with seed interactions. It is, of course, possible that the nonseed, motif interactions have additional functions, e.g., in attracting regulatory factors or switching effector pathways.

Overall, we show that noncanonical miRNA-mRNA targeting is much more widespread than anticipated. Moreover, the analysis of base-pairing patterns and of miRNA-binding site motifs indicates that individual miRNAs systematically differ in their target binding modes. Indeed, even members of the same miRNA family can manifest distinct base-pairing patterns. This was previously predicted by RepTar (Elefant et al., 2011) and was observed on a small scale in the analysis of enriched 6-mers in mRNAs recovered in AGO-immunoprecipitates following miRNA transfection (Nelson et al., 2011; Wang et al., 2010).

The recently published human AGO2 crystal structure (Elkayam et al., 2012) does not exclude the possibility of noncanonical seed interactions. The trajectory of the miRNA seen in the structure leaves most base edges accessible to be read by potential target molecules. Biochemical studies show that the structure of hAGO2 is flexible, and miRNA binding stabilizes and spatially orients AGO2 domains. Differences in patterns of miRNA-target RNA base pairing can induce allosteric changes in the RISC complex, potentially leading to different AGO

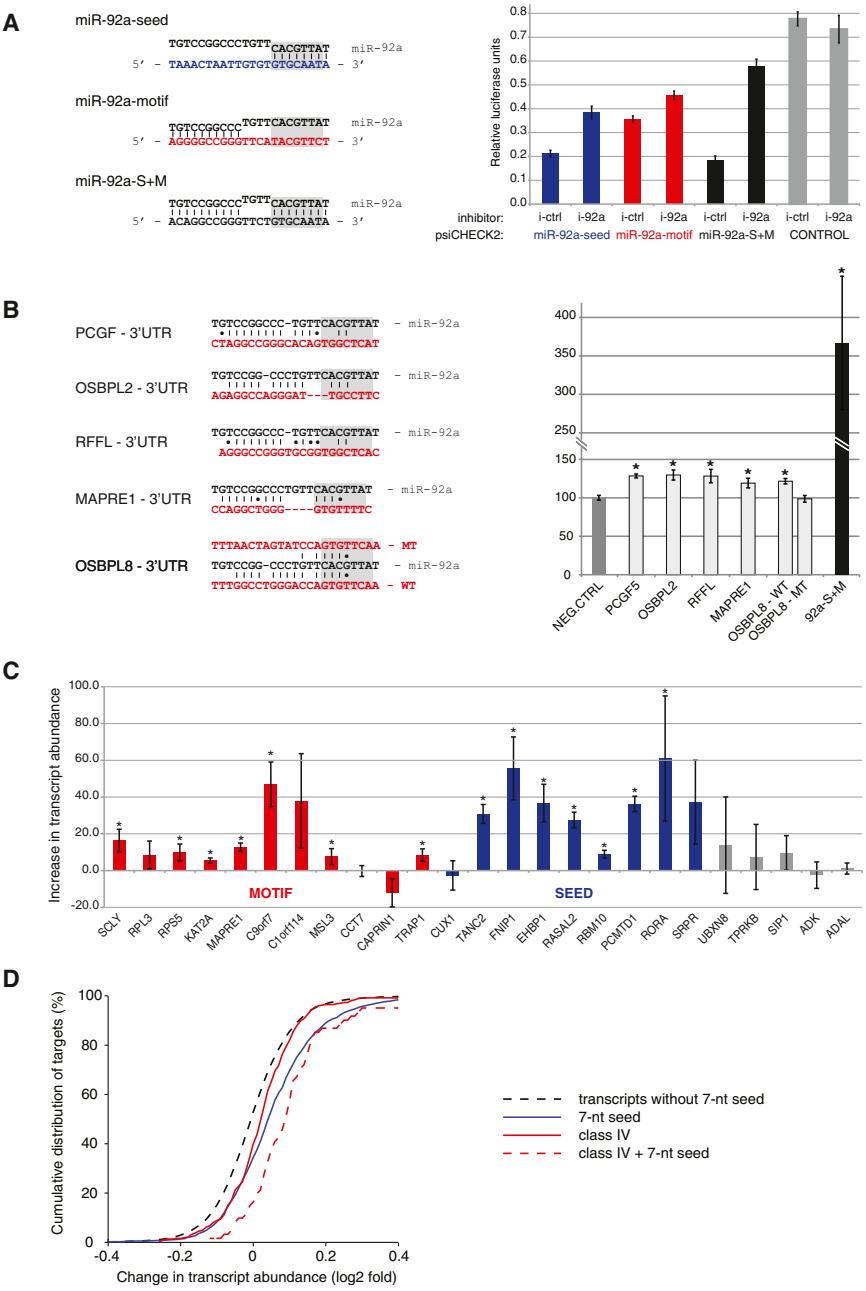


**Figure 5. Experimental Validation of Noncanonical Interactions**

(A) Reporter vectors were constructed by inserting miR-92a-binding sites matching the seed, 3′ motif, or seed+3′ motif (S+M) (left) into the 3′ UTR of *Renilla* luciferase in a psiCHECK2 vector. *Renilla* to firefly luciferase ratios are shown with error bars representing SE from four independent experiments (right). All binding sites caused miR-92-dependent downregulation of luciferase expression ($p < 0.05$, t test).

(B) Reporter vectors were constructed by inserting 3′ UTRs of identified class IV miR-92a targets into the 3′ UTR of *Renilla* luciferase in a psiCHECK2 vector. Mean changes in *Renilla* to firefly luciferase ratios upon treatment with miR-92a inhibitors are shown with error bars representing SE from at least three independent experiments (right). A schematic of the CLASH identified miR-92a-binding sites within those UTRs, and sites of mutagenesis within one of the reporters are depicted on the left. All wild-type-binding sites resulted in significant increase of Renilla luciferase signal ($p < 0.05$, t test, marked with an asterisk), and mutagenesis of identified binding site resulted in reverting this effect.

(C) Experimental validation of selected CLASH targets with miR-92a seed-only binding sites (blue), miR-92a motif-only binding sites (red), or negative controls (gray). Increase in transcript abundance upon inhibition of endogenous miR-92a was quantified by qRT-PCR and internally normalized to GAPDH. The bars represent the average from three independent experiments, error bars represent SD, and samples with $p < 0.05$ (t test) are marked with an asterisk.

(D) Changes in mRNA abundance upon miR-92a depletion in cells measured by microarrays. The graph shows a cumulative distribution of the log2 fold change (LFC) of mRNA abundance for various kinds of miR-92a targets. Transcripts without 7-mer seed serve as negative control.

See also Figure S5.

activities. This suggests that the various interaction classes and/or the specific motifs identified might have distinct functional roles. The integration of CLASH data with RNA-sequencing and proteomics should give a clearer indication of the range of miRNA functions and their relationship to miRNA-mRNA interaction patterns.

Many interactions between Argonaute proteins and abundant, stable rRNA and tRNA species can be found in our data and in published high-throughput AGO-CLIP experiments (Chi et al., 2009; Hafner et al., 2010a). Evidence for miRNA-rRNA interactions has been reported, including the association of miR-206 with both nuclear preribosomes and mature cytoplasmic ribosomes (Politz et al., 2006). miR-206 is, however, specific for skeletal muscles and is not expressed in HEK293 cells. In addition, the involvement of AGO2 in pre-rRNA processing has been reported, although it is unclear whether this is dependent on the RISC pathway (Liang and Crooke, 2011). Specific, short tRNA fragments can be bound by AGO proteins and possibly function analogously to miRNAs (Burroughs et al., 2011), but there are no previous reports of tRNAs being targeted by miRNAs.

It was recently proposed that "competing endogenous RNA" (ceRNA), generated from transcribed pseudogenes and long noncoding RNAs, participates in mRNA regulation by competing for miRNA binding (Salmena et al., 2011). We speculate that regulation by competition for miRNAs involves not only ncRNAs and other modestly expressed species but also the abundant stable RNAs. In some cases, the highly abundant tRNAs and

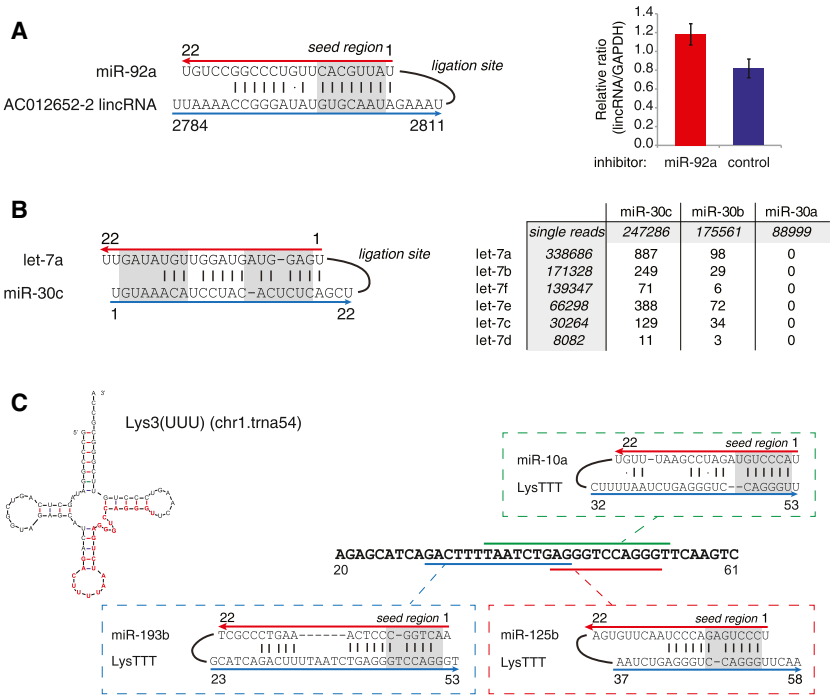


| | miR-30c | miR-30b | miR-30a |
|---|---|---|---|
| | *single reads* | *247286* | *175561* | *88999* |
| let-7a | *338686* | 887 | 98 | 0 |
| let-7b | *171328* | 249 | 29 | 0 |
| let-7f | *139347* | 71 | 6 | 0 |
| let-7e | *66298* | 388 | 72 | 0 |
| let-7c | *30264* | 129 | 34 | 0 |
| let-7d | *8082* | 11 | 3 | 0 |

| miRNA | sequence alignment | seed | number of chimeras with LysTTT |
|---|---|---|---|
| miR-193b | aactggccctcaagtccgct--------- | actggcc | 66 |
| miR-10a | ----taccctgt-agatccg--aatttgtg- | accctgt | 406 |
| miR-10b | ----taccctgt-agaaccg--aatttgtg- | accctgt | 83 |
| miR-125b | -----tccctg--agacct--aacttgtga | ccctgag | 309 |
| miR-125a-5p | -----tccctg--agaccctttaacctgtga | ccctgag | 62 |

**Figure 6. Examples of Interactions between miRNAs and Non-mRNA Targets**

(A) Experimentally validated, reproducible interaction between miR-92a and lincRNA AC012652-2 with canonical seed match. Change in the expression level of the lincRNA upon miR-92a inhibition was estimated by qRT-PCR. The error bar represents SE from three biological replicate experiments.

(B) Putative interaction between miR-30 and let-7; left, folded structure of miR-30c- let-7a chimera; right, numbers of chimeras supporting the interactions between pairs of let-7 and miR-30 family members. The specificity of the interaction is supported by the presence of multiple chimeras between let-7 and miR-30b/c, and the absence of chimeras between let-7 and miR-30a.

(C) Putative interactions between miRNAs and $tRNA^{Lys3(UUU)}$. miR-10a, miR-10b, miR-125b, miR-125a-5p, and miR-193b bind with high reproducibility to the same region of $tRNA^{Lys3(UUU)}$, marked red on the tRNA structure (chr1.trna54). As shown in the sequence alignment, these miRNAs have different seed sequences but are similar overall.

See also Data S3.

rRNAs may also "buffer" miRNAs. They might potentially bind miRNAs that are in (perhaps temporary) excess over cognate targets, preventing inappropriate target binding and/or protecting unbound miRNAs against premature degradation. This model is supported by the observation that miRNA interactions with mRNAs have a lower average free energy than those with stable RNA species (data not shown), so authentic target mRNAs might readily recruit cognate miRNAs from the buffered pool.

Interactions between pairs of distinct miRNAs were not very frequent (~3%), but some were highly reproducible and apparently isoform specific—for example, miR-30::let-7. Two published reports of miRNA-miRNA interactions reveal different outcomes. Binding of miR-107 and let-7 mutually reduced miRNA stability and activity (Chen et al., 2011), whereas binding of miR-709 alters the biogenesis of miR-15a/16-1 (Tang et al., 2012).

The application of the CLASH technique to miRNAs offers many possibilities for future research. As an example, analyses of miRNA association reveal comparable distributions of miRNAs associated with the four mammalian AGO homologs (Burroughs et al., 2011; Liu et al., 2004; Meister et al., 2004; Su et al., 2009), but it is less clear whether all miRNAs target the same mRNAs when bound to different AGOs. Similarly, closely related paralogs exist for many human miRNAs, but it has been difficult to determine their relative efficiencies in mRNA targeting. The distribution of nontemplated terminal U residues among miRNAs has also been determined (Kim et al., 2010), but not how this effects targeting in vivo. More generally, the spectrum of miRNA-mRNA interactions is expected to rapidly change during differentiation, and viral infection and following metabolic shifts or environmental insults. All of these can potentially be addressed using CLASH.

## EXPERIMENTAL PROCEDURES

### CLASH Analyses

The previously reported protocol (Kudla et al., 2011) was extensively modified to allow miRNA target identification in mammalian cells. The experimental protocol, variants tested, and bioinformatic analyses are described in detail in the Supplemental Information.

### Cell Lines

A protein A-TEV protease cleavage site 6xHis (PTH) tag was fused to the N terminus of human AGO1 and stably transfected into Flp-In T-REx 293 cells. PTH-AGO1 expression was induced with Doxycycline and confirmed by western blotting.

### Experimental Validation of CLASH Targets

Flp-In T-REx 293-hAGO1 cells were transfected with miR-92a inhibitor or universal negative control. 48 hr posttransfection RNA was isolated, and cDNA was quantified using primers listed in Table S6. Luciferase reporter vectors were prepared by cloning short oligonucleotides containing single miR-92a-binding sites or PCR-amplified long fragments of 3′ UTRs (sequences in Table S6) into the 3′ UTR of *Renilla* luciferase in the psiCHECK2 vector (Promega). HEK293 cells were transfected in 96-well plates with reporter vectors or nonmodified psiCHECK2 as control together with control or miR-92a inhibitors. Luminescence of *Renilla* and firefly (internal reference) luciferases was measured 48 hr posttransfection.

## ACCESSION NUMBERS

The GEO accession number for the microarray data reported in this paper is GSE46039.

## SUPPLEMENTAL INFORMATION

Supplemental Information includes Extended Experimental Procedures, five figures, three data files, and six tables and can be found with this article online at http://dx.doi.org/10.1016/j.cell.2013.03.043.

## ACKNOWLEDGMENTS

We thank Amy Buck and Gracjan Michlewski for critical comments on the manuscript, Sander Granneman for helpful technical suggestions, Guido Sanguinetti and members of the Tollervey lab for discussions, and Ricardo Almeida and Markus Bohnsack for vectors. This work was supported by Wellcome Trust grants to D.T. (077248) and G.K. (097383). Work in the in the Wellcome Trust Centre for Cell Biology is supported by Wellcome Trust core funding (092076). A.H., G.K., T.D., and D.T. designed the experiments; A.H. and T.D. performed experiments; A.H., G.K., and D.T. analyzed the data; and A.H., G.K., and D.T. wrote the paper.

Received: July 4, 2012
Revised: December 21, 2012
Accepted: March 20, 2013
Published: April 25, 2013

## REFERENCES

Altschul, S.F., Gish, W., Miller, W., Myers, E.W., and Lipman, D.J. (1990). Basic local alignment search tool. J. Mol. Biol. *215*, 403–410.

Bailey, T.L., and Elkan, C. (1994). Fitting a mixture model by expectation maximization to discover motifs in biopolymers. Proceedings of the Second International Conference on Intelligent Systems for Molecular Biology, 28–36.

Barat, C., Lullien, V., Schatz, O., Keith, G., Nugeyre, M.T., Grüninger-Leitch, F., Barré-Sinoussi, F., LeGrice, S.F., and Darlix, J.L. (1989). HIV-1 reverse transcriptase specifically interacts with the anticodon domain of its cognate primer tRNA. EMBO J. *8*, 3279–3285.

Bartel, D.P. (2009). MicroRNAs: target recognition and regulatory functions. Cell *136*, 215–233.

Broderick, J.A., Salomon, W.E., Ryder, S.P., Aronin, N., and Zamore, P.D. (2011). Argonaute protein identity and pairing geometry determine cooperativity in mammalian RNA silencing. RNA *17*, 1858–1869.

Burroughs, A.M., Ando, Y., de Hoon, M.J., Tomaru, Y., Suzuki, H., Hayashizaki, Y., and Daub, C.O. (2011). Deep-sequencing of human Argonaute-associated small RNAs provides insight into miRNA sorting and reveals Argonaute association with RNA fragments of diverse origin. RNA Biol. *8*, 158–177.

Chatterjee, S., and Grosshans, H. (2009). Active turnover modulates mature microRNA activity in Caenorhabditis elegans. Nature *461*, 546–549.

Chen, P.S., Su, J.L., Cha, S.T., Tarn, W.Y., Wang, M.Y., Hsu, H.C., Lin, M.T., Chu, C.Y., Hua, K.T., Chen, C.N., et al. (2011). miR-107 promotes tumor progression by targeting the let-7 microRNA in mice and humans. J. Clin. Invest. *121*, 3442–3455.

Chi, S.W., Zang, J.B., Mele, A., and Darnell, R.B. (2009). Argonaute HITS-CLIP decodes microRNA-mRNA interaction maps. Nature *460*, 479–486.

Chi, S.W., Hannon, G.J., and Darnell, R.B. (2012). An alternative mode of microRNA target recognition. Nat. Struct. Mol. Biol. *19*, 321–327.

Elefant, N., Altuvia, Y., and Margalit, H. (2011). A wide repertoire of miRNA binding sites: prediction and functional implications. Bioinformatics *27*, 3093–3101.

Elkayam, E., Kuhn, C.D., Tocilj, A., Haase, A.D., Greene, E.M., Hannon, G.J., and Joshua-Tor, L. (2012). The structure of human argonaute-2 in complex with miR-20a. Cell *150*, 100–110.

Fabian, M.R., Sonenberg, N., and Filipowicz, W. (2010). Regulation of mRNA translation and stability by microRNAs. Annu. Rev. Biochem. *79*, 351–379.

Garcia, D.M., Baek, D., Shin, C., Bell, G.W., Grimson, A., and Bartel, D.P. (2011). Weak seed-pairing stability and high target-site abundance decrease the proficiency of lsy-6 and other microRNAs. Nat. Struct. Mol. Biol. *18*, 1139–1146.

Grant, C.E., Bailey, T.L., and Noble, W.S. (2011). FIMO: scanning for occurrences of a given motif. Bioinformatics *27*, 1017–1018.

Grey, F., Tirabassi, R., Meyers, H., Wu, G., McWeeney, S., Hook, L., and Nelson, J.A. (2010). A viral microRNA down-regulates multiple cell cycle genes through mRNA 5'UTRs. PLoS Pathog. *6*, e1000967.

Grimson, A., Farh, K.K., Johnston, W.K., Garrett-Engele, P., Lim, L.P., and Bartel, D.P. (2007). MicroRNA targeting specificity in mammals: determinants beyond seed pairing. Mol. Cell *27*, 91–105.

Ha, I., Wightman, B., and Ruvkun, G. (1996). A bulged lin-4/lin-14 RNA duplex is sufficient for Caenorhabditis elegans lin-14 temporal gradient formation. Genes Dev. *10*, 3041–3050.

Hafner, M., Landthaler, M., Burger, L., Khorshid, M., Hausser, J., Berninger, P., Rothballer, A., Ascano, M., Jr., Jungkamp, A.C., Munschauer, M., et al. (2010a). Transcriptome-wide identification of RNA-binding protein and microRNA target sites by PAR-CLIP. Cell *141*, 129–141.

Hafner, M., Landthaler, M., Burger, L., Khorshid, M., Hausser, J., Berninger, P., Rothballer, A., Ascano, M., Jungkamp, A.C., Munschauer, M., et al. (2010b). PAR-CliP—a method to identify transcriptome-wide the binding sites of RNA binding proteins. J. Vis. Exp. *41*, 2034.

Hansen, T.B., Jensen, T.I., Clausen, B.H., Bramsen, J.B., Finsen, B., Damgaard, C.K., and Kjems, J. (2013). Natural RNA circles function as efficient microRNA sponges. Nature *495*, 384–388.

Hsu, S.D., Lin, F.M., Wu, W.Y., Liang, C., Huang, W.C., Chan, W.L., Tsai, W.T., Chen, G.Z., Lee, C.J., Chiu, C.M., et al. (2011). miRTarBase: a database curates experimentally validated microRNA-target interactions. Nucleic Acids Res. *39*(Database issue), D163–D169.

John, B., Enright, A.J., Aravin, A., Tuschl, T., Sander, C., and Marks, D.S. (2004). Human microRNA targets. PLoS Biol. *2*, e363.

Kertesz, M., Iovino, N., Unnerstall, U., Gaul, U., and Segal, E. (2007). The role of site accessibility in microRNA target recognition. Nat. Genet. *39*, 1278–1284.

Kim, Y.K., Heo, I., and Kim, V.N. (2010). Modifications of small RNAs and their associated proteins. Cell *143*, 703–709.

Krek, A., Grün, D., Poy, M.N., Wolf, R., Rosenberg, L., Epstein, E.J., MacMenamin, P., da Piedade, I., Gunsalus, K.C., Stoffel, M., and Rajewsky, N. (2005). Combinatorial microRNA target predictions. Nat. Genet. *37*, 495–500.

Kudla, G., Granneman, S., Hahn, D., Beggs, J., and Tollervey, D. (2011). Cross-linking, ligation, and sequencing of hybrids reveals RNA-RNA interactions in yeast. Proc. Natl. Acad. Sci. USA *108*, 10010–10015.

Lal, A., Navarro, F., Maher, C.A., Maliszewski, L.E., Yan, N., O'Day, E., Chowdhury, D., Dykxhoorn, D.M., Tsai, P., Hofmann, O., et al. (2009). miR-24 Inhibits cell proliferation by targeting E2F2, MYC, and other cell-cycle genes via binding to "seedless" 3'UTR microRNA recognition elements. Mol. Cell *35*, 610–625.

Lewis, B.P., Burge, C.B., and Bartel, D.P. (2005). Conserved seed pairing, often flanked by adenosines, indicates that thousands of human genes are microRNA targets. Cell *120*, 15–20.

Li, Y., Zhang, M., Chen, H., Dong, Z., Ganapathy, V., Thangaraju, M., and Huang, S. (2010). Ratio of miR-196s to HOXC8 messenger RNA correlates with breast cancer cell migration and metastasis. Cancer Res. *70*, 7894–7904.

Lian, S.L., Li, S., Abadal, G.X., Pauley, B.A., Fritzler, M.J., and Chan, E.K. (2009). The C-terminal half of human Ago2 binds to multiple GW-rich regions of GW182 and requires GW182 to mediate silencing. RNA *15*, 804–813.

Liang, X.H., and Crooke, S.T. (2011). Depletion of key protein components of the RISC pathway impairs pre-ribosomal RNA processing. Nucleic Acids Res. *39*, 4875–4889.

Liu, J., Carmell, M.A., Rivas, F.V., Marsden, C.G., Thomson, J.M., Song, J.J., Hammond, S.M., Joshua-Tor, L., and Hannon, G.J. (2004). Argonaute2 is the catalytic engine of mammalian RNAi. Science *305*, 1437–1441.

Markham, N.R., and Zuker, M. (2008). UNAFold: software for nucleic acid folding and hybridization. Methods Mol. Biol. *453*, 3–31.

Meister, G., Landthaler, M., Patkaniowska, A., Dorsett, Y., Teng, G., and Tuschl, T. (2004). Human Argonaute2 mediates RNA cleavage targeted by miRNAs and siRNAs. Mol. Cell *15*, 185–197.

Memczak, S., Jens, M., Elefsinioti, A., Torti, F., Krueger, J., Rybak, A., Maier, L., Mackowiak, S.D., Gregersen, L.H., Munschauer, M., et al. (2013). Circular RNAs are a large class of animal RNAs with regulatory potency. Nature *495*, 333–338.

Nelson, P.T., Wang, W.X., Mao, G., Wilfred, B.R., Xie, K., Jennings, M.H., Gao, Z., and Wang, X. (2011). Specific sequence determinants of miR-15/107 microRNA gene group targets. Nucleic Acids Res. *39*, 8163–8172.

Poliseno, L., Salmena, L., Zhang, J., Carver, B., Haveman, W.J., and Pandolfi, P.P. (2010). A coding-independent function of gene and pseudogene mRNAs regulates tumour biology. Nature *465*, 1033–1038.

Politz, J.C., Zhang, F., and Pederson, T. (2006). MicroRNA-206 colocalizes with ribosome-rich regions in both the nucleolus and cytoplasm of rat myogenic cells. Proc. Natl. Acad. Sci. USA *103*, 18957–18962.

Pollard, K.S., Hubisz, M.J., Rosenbloom, K.R., and Siepel, A. (2010). Detection of nonneutral substitution rates on mammalian phylogenies. Genome Res. *20*, 110–121.

Reczko, M., Maragkakis, M., Alexiou, P., Grosse, I., and Hatzigeorgiou, A.G. (2012). Functional microRNA targets in protein coding sequences. Bioinformatics *28*, 771–776.

Rehmsmeier, M., Steffen, P., Hochsmann, M., and Giegerich, R. (2004). Fast and effective prediction of microRNA/target duplexes. RNA *10*, 1507–1517.

Salmena, L., Poliseno, L., Tay, Y., Kats, L., and Pandolfi, P.P. (2011). A ceRNA hypothesis: the Rosetta Stone of a hidden RNA language? Cell *146*, 353–358.

Shin, C., Nam, J.W., Farh, K.K., Chiang, H.R., Shkumatava, A., and Bartel, D.P. (2010). Expanding the microRNA targeting code: functional sites with centered pairing. Mol. Cell *38*, 789–802.

Su, H., Trombly, M.I., Chen, J., and Wang, X. (2009). Essential and overlapping functions for mammalian Argonautes in microRNA silencing. Genes Dev. *23*, 304–317.

Tang, R., Li, L., Zhu, D., Hou, D., Cao, T., Gu, H., Zhang, J., Chen, J., Zhang, C.Y., and Zen, K. (2012). Mouse miRNA-709 directly regulates miRNA-15a/16-1 biogenesis at the posttranscriptional level in the nucleus: evidence for a microRNA hierarchy system. Cell Res. *22*, 504–515.

Vella, M.C., Reinert, K., and Slack, F.J. (2004). Architecture of a validated microRNA:target interaction. Chem. Biol. *11*, 1619–1623.

Wang, W.X., Wilfred, B.R., Xie, K., Jennings, M.H., Hu, Y.H., Stromberg, A.J., and Nelson, P.T. (2010). Individual microRNAs (miRNAs) display distinct mRNA targeting "rules". RNA Biol. *7*, 373–380.

Yekta, S., Shih, I.H., and Bartel, D.P. (2004). MicroRNA-directed cleavage of HOXB8 mRNA. Science *304*, 594–596.

Zhang, C., and Darnell, R.B. (2011). Mapping in vivo protein-RNA interactions at single-nucleotide resolution from HITS-CLIP data. Nat. Biotechnol. *29*, 607–614.